

Collinear laser spectroscopy on the ground state and an excited state in neutral ^{55}Mn A. Klose,^{1,2} K. Minamisono,^{2,3} and P. F. Mantica^{1,2}¹*Department of Chemistry, Michigan State University, East Lansing, Michigan 48824, USA*²*National Superconducting Cyclotron Laboratory, Michigan State University, East Lansing, Michigan 48824, USA*³*Department of Physics and Astronomy, Michigan State University, East Lansing, Michigan 48824, USA*

(Received 8 July 2013; published 7 October 2013)

Collinear laser spectroscopy was performed on an atomic beam of stable ^{55}Mn . An ion beam of $^{55}\text{Mn}^+$ was generated in an ion source, accelerated to 15 keV, and neutralized via charge-exchange reactions with a Na vapor. A long-lived metastable state of Mn I, near-resonantly populated in the charge-exchange process, was investigated via laser probing in addition to a laser excitation from the ground state in Mn I. The relative population of the Mn I metastable state compared to that of the ground state was found to be 0.7 ± 0.3 . A theoretical calculation, which included feeding to the ground state and the metastable state from higher-energy excited electronic states populated in the charge-exchange process, agreed with the present result. The deduced A and B hyperfine coupling constants agreed with literature values, where available.

DOI: [10.1103/PhysRevA.88.042701](https://doi.org/10.1103/PhysRevA.88.042701)

PACS number(s): 34.70.+e, 32.10.Fn, 42.62.Fi

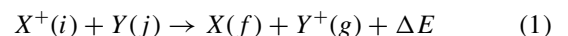
I. INTRODUCTION

Collinear laser spectroscopy (CLS) [1] is a well-developed technique to measure hyperfine (HF) spectra. CLS relies on the co-propagation of continuous-wave (cw) laser light with an ionic or atomic beam with tens of keV total kinetic energy. Laser-induced fluorescence emitted from the ionic or atomic beam is measured as a function of laser frequency. One major advantage of the collinear geometry of the laser light and ion or atom beam is Doppler compression of the laser-induced fluorescence profile of an electronic transition when ions are accelerated using a well-defined electrostatic potential [2]. While laser excitation from the ground state of the singly ionized species using a commercial narrow-bandwidth continuous-wave laser system (200–1000 nm) may be possible for some elements, the electronic structure of the corresponding neutral species provides complementary and/or extending selection of transition frequencies for laser-spectroscopy studies. An ion beam can be converted into an atomic beam via charge-exchange reactions with a suitable alkali-metal vapor [3–6] so that the atomic structure of the neutral species can be exploited for the selection of transition frequencies. The distribution of electronic states populated in the charge-exchange reactions is dependent on the first ionization energies of both the alkali-metal vapor and incident ion. Long-lived metastable states that have near-resonant charge transfer with the ground state of the alkali-metal atom may be preferentially populated in the charge-exchange reactions. The metastable states populated in the charge-exchange reactions may be used as the initial state for a laser excitation in species where excitation from the ground state is difficult. Laser spectroscopy from metastable states populated in charge-exchange reactions has been exploited in noble gases [7] where the level density is sparse. In contrast, the level density of many other species, such as first row transition elements, is much higher. The population of the outgoing atomic beam may be fragmented across many levels, but the increased number of levels is thought to provide a corresponding increase in suitable laser-excitation schemes and a high relative population for near-resonant states.

CLS was used in the present studies to probe both the ground state and a metastable state in ^{55}Mn I populated in charge-exchange reactions of a 15-keV beam of Mn^+ with a Na vapor. A laser probing from the electronic ground state of Fe I populated via charge exchange of a 15-keV $^{56}\text{Fe}^+$ ion beam with Na vapor was also performed. The Fe I CLS measurement served as a baseline measurement of the experimental apparatus. The ^{56}Fe atomic system has zero nuclear spin and therefore exhibits no hyperfine splitting, thus spectroscopy of a particular fine-structure transition has a single peak, providing an ideal case for the analysis of the transition frequency and linewidth. The goal of the present work was to determine the relative population of multiple states in the Mn atomic beam populated in charge-exchange reactions with a Na vapor, as well as investigating the effect of the charge-exchange process on the laser-induced fluorescence line shape of the atomic beam. Atomic-charge exchange processes are discussed in Sec. II, and the experimental setup is described in Sec. III. The results and discussion are presented in Sec. IV followed by a summary in Sec. V.

II. ATOMIC CHARGE EXCHANGE IN CLS

The charge-exchange process of



is considered here, where $X^+(i)$ is the incident ion in electronic state i , Y is the alkali-metal atom in state j , $X(f)$ is the outgoing atom in state f , $Y^+(g)$ is the alkali-metal ion in state g , and ΔE is the energy defect of the reaction. When $\Delta E = 0$, the charge-exchange process is referred to as a resonant process. If $\Delta E \neq 0$, the energy defect is given or taken from the kinetic energy of the ionic or atomic beam. In particular, when $\Delta E < 0$, the outgoing atomic beam gains energy, broadening the energy distribution of the beam by a maximum of ΔE . On the other hand, when $\Delta E > 0$, energy is required for the charge-exchange process to occur and the energy is taken from the kinetic energy of the incident ion beam. Some excited electronic states populated in the charge-exchange reactions will have prompt decay to lower-energy states (e.g., the ground state) while others are long-lived metastable states (e.g.,

$\tau > 100 \mu\text{s}$). These charge-exchange processes can affect the velocity distribution of the atomic beam whereby the laser-induced fluorescence line shape is broadened and may become asymmetric. A Voigt profile, which is a convolution of Lorentzian and Gaussian functions, can be employed to reproduce the distorted resonance lineshape. The Voigt profile is a symmetric function, and does not account for asymmetric broadening mechanisms. The asymmetry from processes that have $\Delta E > 0$ can be quantitatively investigated in cases where sparse, well-separated inelastic channels are available and symmetric profiles can be fitted for each charge-exchange channel [5,6]. On the other hand, species that have a high level density such as transition metals necessitate a phenomenological asymmetric line shape to account for the inelastic processes. The asymmetric line shape can be modeled by varying the linewidth of the profile exponentially from the centroid, v_c , [8] as

$$\Gamma(v) = \frac{2\Gamma_0}{1 + \exp[a(v - v_c)]}, \quad (2)$$

where Γ_0 is the unperturbed linewidth and a is the asymmetry parameter. For $a = 0$, the frequency-dependent width simplifies to $\Gamma(v) = \Gamma_0$.

Semiclassical time-dependent perturbation theory can be used to calculate the cross section for charge exchange of ion beams with tens of keV total kinetic energy with a thermal gas [9–11]. The theory of Rapp and Francis [11] offers one approach, where the cross section for the charge-exchange process is numerically calculated as a function of the velocity of the incident ion, the average ionization potential of X and Y , and ΔE . In general, the cross section for charge exchange is inversely related to ΔE , implying that atomic states that are near-resonant have enhanced cross sections compared to inelastic processes.

III. EXPERIMENTAL PROCEDURE

The experiments were conducted using the CLS system of the beam cooler and laser spectroscopy (BECOLA) facility [12] at the National Superconducting Cyclotron Laboratory (NSCL) at Michigan State University. Singly charged ion beams were generated in an ion source described in Sec. III A. The ion source was placed on a voltage of 15 kV relative to ground potential. Ions were extracted from the source and accelerated to the CLS beam line, which was on ground potential. The ion beam was deflected 30° and collinearly propagated with single-mode cw laser light. The ion beam was neutralized via charge-exchange reactions with a Na vapor in a charge-exchange cell (CEC) [6]. The CEC was placed on a variable voltage to adjust the velocity of the ion beam prior to the charge-exchange reactions, as a means of Doppler shifting the laser frequency experienced by the atomic beam. The differential Doppler shift of the laser frequency experienced by the atomic beam is given as

$$\frac{\delta v'}{\delta U} \approx \frac{ve}{\sqrt{2eUm}c^2}, \quad (3)$$

where δU is the change in the total acceleration voltage and $\delta v'$ is the differential change in the laser frequency experienced by the atomic beam. Laser-induced fluorescence from the atomic

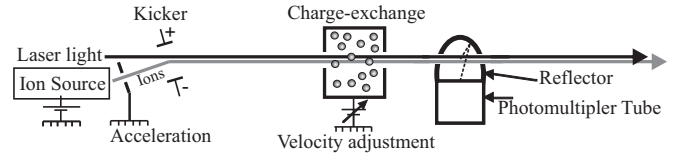


FIG. 1. Schematic of the collinear laser spectroscopy experimental setup. Ions were produced and accelerated to 15 keV, deflected 30° , and neutralized via charge exchange with a Na vapor. Laser light was co-propagated with the atomic beam and laser-induced fluorescence was collected by a reflector and detected by a photomultiplier tube. The dashed lines represent laser-induced fluorescence emitted from the atomic beam and reflected to the photomultiplier tube.

beam was detected at each ion-beam velocity step using an ellipsoidal reflector and photomultiplier tube [12,13] placed ~ 30 cm downstream of the CEC. A schematic diagram of the experimental setup is shown in Fig. 1.

A. Production and acceleration of the ion beams

Singly charged ions of Fe^+ and Mn^+ were produced by electron bombardment of bis(cyclopentadienyl) iron (II) (ferrocene) and bis(cyclopentadienyl) manganese (II) (manganocene), respectively. The ferrocene or manganocene vapor was separately introduced into the ion source chamber using the metal ions from volatile organometallic compounds (MIVOC) technique [14,15]. The MIVOC chamber was operated at temperatures ranging 20–100 $^\circ\text{C}$.

The ion source was modeled after the ionizer used in a Stanford Research Systems residual gas analyzer [16]. The ion source consisted of a negatively biased filament surrounding a cylindrical grid which served as the anode. Electrons emitted from the filament were accelerated to 125 eV and passed through the anode grid. Some fraction of the gaseous atoms and molecules inside of the anode grid were ionized by the electrons and extracted out of the anode volume using a negatively biased extraction plate. The variation in the kinetic energy of the extracted ions was less than 1 eV. After extraction, the ions were accelerated to the CLS beam line. The diameter of the ion beam was defined using apertures at the beginning and end of the CLS beam line. The apertures had a diameter of 5 mm, and the typical beam current passing through the CLS beam line was between 1 and 10 nA. The intensity of Mn^+ or Fe^+ in the total ion-beam current was $\sim 10\%$.

B. Charge exchange

The 15-keV ion beam was passed through the CEC, where some fraction of the beam was neutralized via charge-exchange reactions with a Na vapor. The density of the alkali-metal vapor was controlled such that 30–50% of the outgoing beam was neutralized. The CEC is described in detail in Ref. [6].

Multiple electronic states in the neutral Mn beam were populated in the charge-exchange reactions. An electronic energy diagram for the two charge-exchange processes of the Na vapor and the Mn^+ beam investigated in this work are depicted in Fig. 2. The first ionization energies of Mn and Na are 7.434 02 and 5.139 08 eV, respectively [17]. An energy change of $\Delta E = -2.294 94$ eV is expected in a Mn^+ beam

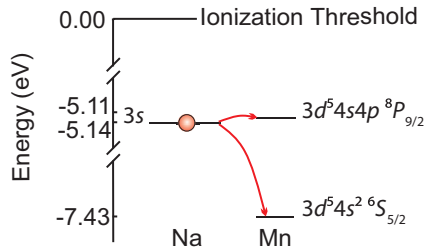


FIG. 2. (Color online) The charge-exchange processes between Na and Mn^+ that were investigated in this work.

from the transfer of an electron from the ground state of Na to the ground state of Mn. The Mn I $3d^5 4s 4p \ ^8P_{9/2}$ level is 2.31909 eV above the Mn I ground state, making this state nearly resonant with the ground state of Na I ($\Delta E = 0.02415$).

The population of the Fe I ground state via charge exchange of a 15-keV Fe^+ beam with the Na vapor was also investigated. The ionization energy of Fe is 7.9024 eV [17], leading to an energy change of $\Delta E = -2.7633$ eV in the transfer of an electron from the ground state in Na I to the ground state in Fe I.

C. Laser excitation

The energy levels of Mn I relevant to the laser excitations employed in this study are presented in Fig. 3. Solid lines represent the laser-excitations used, and the dashed lines indicate the major de-excitation branches. One of the electronic excitations explored in Mn I was between the $3d^5 4s^2 \ ^6S_{5/2} \rightarrow 3d^5 4s 4p \ ^6P_{7/2}$ levels at a wavelength of 403.19 nm, where the ground state is represented by the $^6S_{5/2}$ term symbol. The other

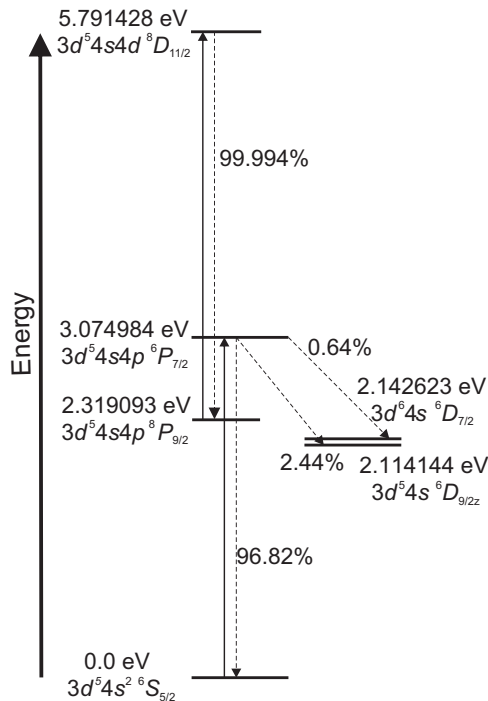


FIG. 3. Partial energy-level diagram of Mn I relevant to the present work. Solid lines indicate laser excitations, and dashed lines represent the de-excitation pathways for fluorescence.

laser excitation was between the $3d^5 4s 4p \ ^8P_{9/2} \rightarrow 3d^5 4s 4d \ ^8D_{11/2}$ states at a wavelength of 357.05 nm, where the lower energy electronic state is a metastable state at 2.31909 eV relative to the ground state. Laser probing of Fe I was achieved by exciting the $3d^6 4s^2 \ ^5D_4$ ground state to the $3d^6 4s 4p \ ^5F_5$ state at 3.33191 eV (372.10 nm).

The laser light used to probe the three transitions was generated by frequency doubling the output of a single-mode cw Ti:sapphire ring laser [12]. The laser power used to probe the atomic beams was of order $100 \mu\text{W}$, and the laser light diameter was (2.5 ± 0.5) mm over the laser and atom interaction region.

IV. RESULTS AND DISCUSSION

A. ^{56}Fe I collinear laser spectroscopy

A typical laser-induced fluorescence spectrum of the Fe I $^5D_4 \rightarrow ^5F_5$ transition is presented in Fig. 4. The ^{56}Fe nucleus has a nuclear spin of zero and therefore exhibits no hyperfine splitting. The fluorescence line shape was fitted with symmetric and asymmetric Voigt profiles described in Sec. II. The reduced χ -squared (χ^2/ν_{df}) values of the fitting result, where ν_{df} is the number of degrees of freedom, were found to be $\chi^2/\nu_{df} = 28$, and $\chi^2/\nu_{df} = 4.3$ for the symmetric and asymmetric Voigt profiles, respectively. The asymmetric Voigt profile provided a better description of the low-energy tail on the fluorescence peak. The centroid of the line shape deduced from the symmetric function was found to be shifted from the centroid of the asymmetric Voigt profile by 1.5 MHz. The deduced centroid obtained using the asymmetric profile is presented in Table I, where the uncertainty in the centroid value had four contributions. The first contribution was the statistical error. The systematic error in the run-to-run variation of the extracted centroid was considered by taking the standard

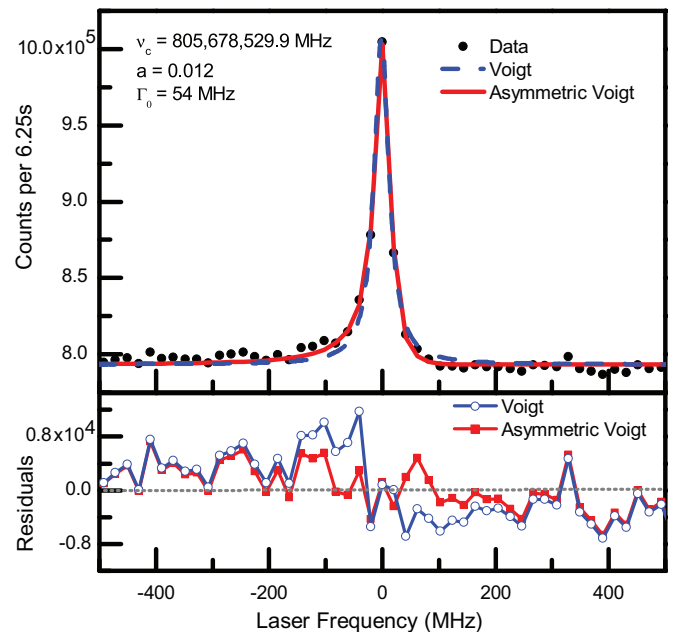


FIG. 4. (Color online) A typical ^{56}Fe I spectrum is presented in the upper panel. Residuals from the symmetric and asymmetric Voigt function fits to the data are displayed in the bottom panel.

TABLE I. The deduced centroid frequency, ν_c , of the Fe I ${}^5D_4 \rightarrow {}^5F_5$ transition investigated.

Present ν_c (MHz)	Literature ν_c (MHz)	Ref.
$805,678,576.0 \pm 0.1 \pm 21 \pm 20.5 \pm 300$	$805,678,680 \pm 30$	[18]

deviation of centroids from 33 data sets and is reported as the second error in Table I. The power supply that was used to define the beam energy had an uncertainty of 1.0 V, corresponding to a 20.5-MHz uncertainty in the centroid frequency (through the differential Doppler shift), and is reported as the third uncertainty. A ± 300 -MHz uncertainty from the helium-neon laser used as a reference for the wavelength measurement [12] added a systematic uncertainty in the laboratory frame laser frequency and is given as the fourth uncertainty. The present values are consistent with the literature values. The impact of the asymmetric line shape on the extracted centroid was negligible in this case, since the overall uncertainty was more than ± 300 MHz and dominated by the uncertainty in the He-Ne laser frequency reference.

The deduced linewidth of the Fe I resonance peak was $\Gamma_0 = (60 \pm 10)$ MHz, a factor of ~ 25 larger than the natural linewidth of 2.58 MHz [18]. The linewidth is broadened mostly by energy transfer in the $\text{Na} + \text{Fe}^+$ charge-exchange reactions. The Fe atom energy distribution was broadened by ~ 2.7 eV in the charge-exchange reaction with the Na vapor. The 2.7-eV kinetic energy spread of the ${}^{56}\text{Fe}$ beam corresponded to a 55-MHz broadening of observed linewidth, consistent with the measured width. Other broadening mechanisms including transient time broadening [19] and laser power broadening [20] were negligible (< 1 MHz).

B. ${}^{55}\text{Mn}$ I hyperfine spectra

Typical HF spectra of the ${}^6S_{5/2} \rightarrow {}^6P_{7/2}$ ground-state laser excitation and the ${}^8P_{9/2} \rightarrow {}^8D_{11/2}$ laser excitation of the metastable state in ${}^{55}\text{Mn}$ ($I_N = 5/2$) are presented in the top panels of Figs. 5 and 6, respectively. The laser frequency is given relative to the deduced center-of-gravity frequencies. Allowed hyperfine transitions are shown in the bottom panels of the figures. All 15 allowed hyperfine transitions for the ground-state excitation and subsequent fluorescence were recorded, and 11 out of the 16 allowed fluorescence peaks were measured for the metastable-state excitation. The five transitions not recorded had the lowest relative intensities due to the spin factor of the hyperfine transition [20] and were not detectable given the sensitivity of the CLS system.

All peaks in a given HF spectrum were simultaneously fitted in terms of the A and B hyperfine coupling constants for each fine level and the center-of-gravity frequency (ν_{cg}) of the HF transitions. Here, A and B are defined as

$$A = \frac{\mu_I \langle H_0 \rangle}{I_N J h} \quad (4)$$

and

$$B = \frac{e Q_s \langle V_{zz} \rangle}{h}, \quad (5)$$

where μ_I is the nuclear magnetic dipole moment, $\langle H_0 \rangle$ is the average magnetic field produced by the atomic electrons

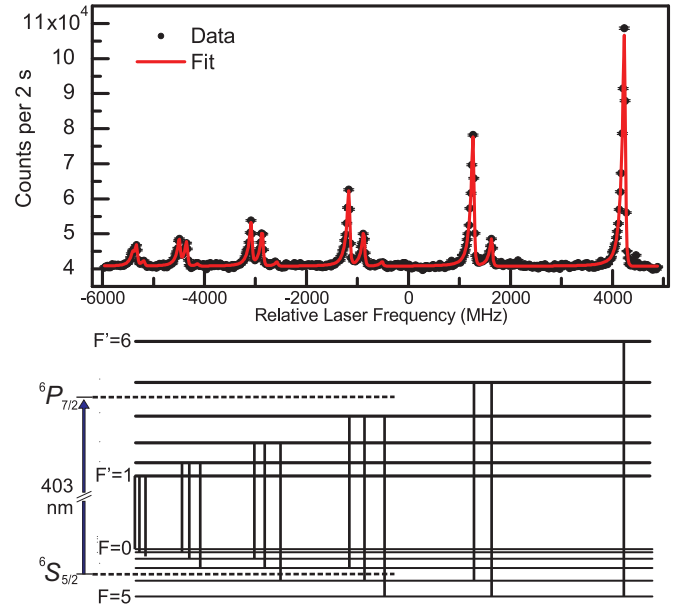


FIG. 5. (Color online) A laser-induced fluorescence spectrum of the ${}^6S_{5/2} \rightarrow {}^6P_{7/2}$ transition in Mn I is presented in the top panel. A schematic of all allowed HF transitions is shown in the bottom panel.

at the nucleus, I_N is the nuclear spin, J is the total angular momentum of the atomic electrons, h is Planck's constant, e is the elementary charge, Q_s is the nuclear spectroscopic quadrupole moment, and $\langle V_{zz} \rangle$ is the average electric-field gradient at the nucleus along the quantization axis. The spectrum was fitted with the asymmetric Voigt profile assuming all peaks had common widths and asymmetry parameters, within a given spectrum. The transition frequency $\nu_{FF'}$ of each

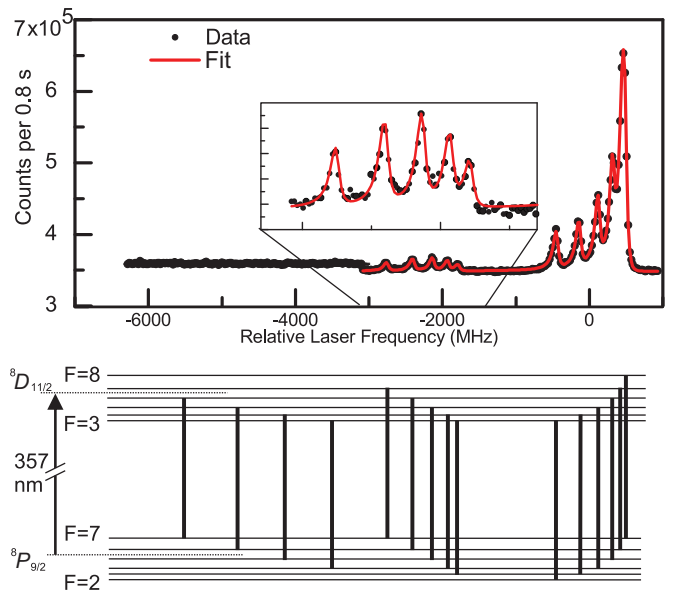


FIG. 6. (Color online) A laser-induced fluorescence spectrum of the ${}^8P_{9/2} \rightarrow {}^8D_{11/2}$ transition in Mn I is presented in the top panel. The spectrum contains two independent data sets over two frequency ranges that overlap at -3000 MHz. A schematic of all allowed HF transitions is shown in the bottom panel.

TABLE II. The center-of-gravity frequency of the transitions in Mn I deduced from the HF spectra. The reported uncertainties are discussed in the text.

Transition	Present ν_{cg} (MHz)	Literature ν_{cg} (MHz)	Ref.
${}^6S_{5/2} \rightarrow {}^6P_{7/2}$	$743,553,074.6 \pm 0.1 \pm 3.7 \pm 19.0 \pm 300$	$743,552,700 \pm 300$	[18]
${}^8P_{9/2} \rightarrow {}^8D_{11/2}$	$839,635,462.6 \pm 0.1 \pm 9.5 \pm 19.0 \pm 300$	$839,635,000 \pm 300$	[18]

$F \rightarrow F'$ transition was given as

$$\nu_{FF'} = \nu_{cg} + \frac{1}{2}[A_U C'(F', I_N, J) - A_L C(F, I_N, J)] + \frac{3}{4}[B_U D(C', I_N, J) - B_L D(C, I_N, J)], \quad (6)$$

where

$$D(C, I_N, J) = \frac{C(C+1) - \frac{4}{3}I_N(I_N+1)J(J+1)}{2I_N(2I_N-1)J(2J-1)} \quad (7)$$

and

$$C(F, I_N, J) = F(F+1) - I_N(I_N+1) - J(J+1). \quad (8)$$

Here, F is the quantum number for hyperfine level ($|I_N - J| < F < |I_N + J|$). The L and U subscripts denote the lower and upper levels of the laser excitation, respectively. The deduced center-of-gravity frequencies for both transitions are listed in Table II and the deduced A and B factors for all four levels investigated are reported in Table III.

The uncertainty in the deduced center-of-gravity frequencies is broken down, in turn from the left, into statistical error, systematic error, beam energy uncertainty, and reference frequency uncertainty. The uncertainty in the deduced A and B hyperfine coupling constants listed in Table III includes the statistical error, listed as the first uncertainty, and systematic error evaluated by analyzing run-to-run variation in the deduced A and B factors, given as the second uncertainty. The ± 300 -MHz uncertainty in the He-Ne laser frequency had negligible contribution to the uncertainties of the deduced A and B constants.

The width, Γ_0 , and asymmetry parameter, a , deduced from the fits to the HF spectrum for both Mn I transitions are presented in Table IV. The differential Doppler shift of the ${}^{55}\text{Mn}$ beam at 15 keV was 19.0 MHz/V, corresponding to a 43-MHz linewidth broadening from the 2.3-eV change in energy. A large portion (47%) of the linewidth broadening of the ground-state transition can be attributed to the 2.3-eV energy gain from the charge-exchange process. The cause

of the additional line broadening is not clear. Neither the natural linewidth nor broadening mechanisms such as laser power broadening or transient time broadening contribute significantly to the overall linewidth. Direct population of the metastable state was a near-resonant charge-exchange process and thus the resonance profile was not broadened due to the charge-exchange energy defect mechanism. The narrow linewidth of the metastable state transition compared to the ground-state transition is an advantage for low count-rate experiments.

The asymmetry in the resonance line shape was a result of inelastic charge-exchange processes. Charge-exchange processes populating levels in Mn I above the ground-state energy of Na requires energy, which is taken from the kinetic energy of the ion beam. Prompt decay of the higher-energy levels to the lower level, which was used for laser excitation, increased the population of the lower level, but asymmetrically increased the velocity distribution of the beam, which was manifested in a low-energy tail in the resonance line shape. Inelastic collisions of the ion or atom beam with Na atoms that excite the Na atoms to higher energy levels create additional asymmetry. The inelastic collisions resulting in excitation of Na atoms could not be separated from inelastic charge-exchange processes of Mn ion or atom because a large number of electronic levels in Mn were populated in the charge-exchange reactions.

A number of excited states populated in the charge-exchange reactions promptly decays ($\tau < 1 \mu\text{s}$) to both the ground and metastable states in Mn I. States with energies of 6 eV or less, relative to the ground state, that promptly decay to the ground and metastable state with more than a 1% branching ratio are summarized in Tables V and VI. Eleven excited states directly feed the ground state compared to four states which promptly decay to the metastable state. The asymmetry of the resonance line shape of the ground-state transition was $(19 \pm 7)\%$ larger compared to the metastable-state transition. The increased asymmetry is attributed to the increased number

TABLE III. The A and B hyperfine coupling constants deduced from the ${}^{55}\text{Mn}$ I HF spectra. The reported uncertainties are discussed in the text.

Level (eV)	Factor	Present (MHz)	Literature (MHz)	Ref.
0.0	A	$-72.5 \pm 0.03 \pm 0.5$	-72.420836 ± 0.000015	[22]
0.0	B	$0.2 \pm 0.3 \pm 1.8$	-0.019031 ± 0.000017	[22]
3.074984	A	$428.2 \pm 0.02 \pm 0.5$	429.16 ± 0.05^a	[23,24]
3.074984	B	$61 \pm 0.3 \pm 2.5$	66.6 ± 1.3^a	[23,24]
2.319093	A	$455.19 \pm 0.09 \pm 0.4$	456 ± 4^a	[7,24]
2.319093	B	$73 \pm 2 \pm 5.5$	48 ± 27	[7]
5.791428	A	$409.4 \pm 0.1 \pm 0.7$	432 ± 11^a	[25,26]
5.791428	B	$-52 \pm 2 \pm 5.5$		

^aWeighted average from multiple references.

TABLE IV. Linewidth and asymmetry of Mn I resonance peaks extracted from the fit discussed in the text.

Transition	Γ_0 (MHz)	a
${}^6S_{5/2} \rightarrow {}^6P_{7/2}$	90 ± 10	0.021 ± 0.001
${}^8P_{9/2} \rightarrow {}^8D_{11/2}$	70 ± 10	0.017 ± 0.001

of $\Delta E > 0$ charge-exchange channels that lead to the ground state compared to those to the metastable state.

C. Relative populations of the Mn I ground and metastable states populated in the Na + Mn⁺ charge-exchange process

The relative populations of the ground state and the ${}^8P_{9/2}$ metastable state at 2.31909 eV populated in the charge-exchange process were deduced from the peak height of the $F = 5 \rightarrow F' = 6$ cyclic transition for the ground state and the $F = 7 \rightarrow F' = 8$ cyclic transition of the metastable state. The initial distribution among m_F (projection of F on the quantization axis) states was assumed to be equal, and the peak height was scaled to reflect the fraction of m_F states. The peak height was also normalized for counting time, laser power, atomic beam current, and the relative intensity of the spin factor for each transition [20].

The normalization for the atomic beam current was sensitive to the fraction of the Mn component in the total beam current. The fraction of ${}^{55}\text{Mn}^+$ in the ion beam extracted from the source was determined by the vapor pressure of the manganocene charge in the MIVOC chamber. The vapor pressure was a function of the chamber temperature; as the temperature increased, the amount of manganocene in the chamber increased exponentially (the Clausius-Clapeyron relation). The increase in the manganocene vapor pressure corresponded to an increase in the amount of Mn⁺ in the extracted ion beam. The normalized resonance signal, ζ , for both transitions are plotted as a function of the MIVOC chamber temperature in Fig. 7. An exponential function

$$\zeta = \alpha \exp[\beta T], \quad (9)$$

where α and β were fit parameters, was used to fit both data sets in Fig. 7. The relative population of the metastable state

TABLE V. Excited electronic states with prompt decay to the Mn I ground state [18,27].

Level (eV)	Term symbol	Branching fraction
0	${}^6S_{5/2}$	
3.072142	${}^6P_{3/2}$	0.970
3.073224	${}^6P_{5/2}$	0.967
3.074984	${}^6P_{7/2}$	0.968
3.843524	${}^4P_{5/2}$	0.288
3.852856	${}^4P_{3/2}$	0.221
4.424846	${}^6P_{3/2}$	0.995
4.429293	${}^6P_{5/2}$	0.994
4.424763	${}^6P_{7/2}$	0.993
5.578349	${}^6P_{7/2}$	0.395
5.598457	${}^6P_{5/2}$	0.454
5.611234	${}^6P_{3/2}$	0.439

TABLE VI. Excited electronic states that promptly decay to the Mn I ${}^8P_{9/2}$ metastable state [18,27].

Level (eV)	Term symbol	Branching fraction
2.319093	${}^8P_{9/2}$	
3.648896	${}^8S_{7/2}$	0.415
5.790901	${}^8D_{7/2}$	0.095
5.791127	${}^8D_{9/2}$	0.384
5.791428	${}^8D_{11/2}$	0.999

compared to the ground state was deduced by taking a ratio of the extracted ζ of the metastable state compared to the ζ of the ground state over the temperature range 325–365 K. The ratio of the populations was found to be

$$\zeta_{\text{metastable}}/\zeta_{\text{ground}} = 0.7 \pm 0.3, \quad (10)$$

where the uncertainty is due to the statistical error of the α and β parameters extracted from the fits as well as the variation of the population ratio as a function of temperature. The ground state of Mn I was populated $\sim 30\%$ more than the metastable state in the charge-exchange reactions and following prompt decays.

The cross sections for populating the two electronic states studied in Mn I through the Na + Mn⁺ atomic charge-exchange reactions were calculated using the theory of Rapp and Francis [11] and the corrections of Dewangan [21]. Results of the calculated charge-exchange cross sections are presented in Table VII. Direct charge-exchange cross sections to the ground state and ${}^8P_{9/2}$ metastable state were calculated along with cross sections for charge-exchange reactions populating fine-structure levels that had $>1\%$ branching to the ground or metastable state. It was assumed that all m_F states were equally populated for charge exchange to a given fine-structure level. The calculated cross sections were scaled by the fraction of decays from a given excited state that populated the $F = 5$ or $F = 7$ level of the ground state or metastable state, respectively.

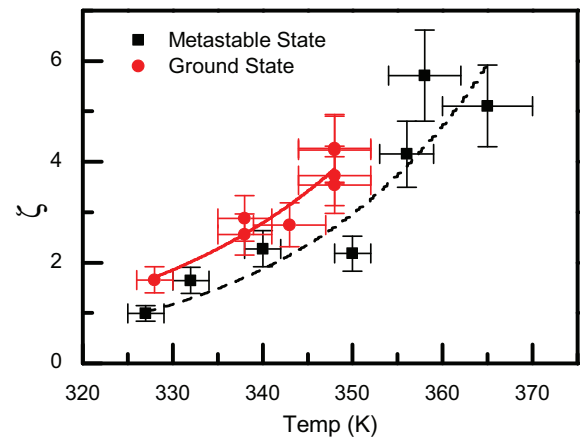


FIG. 7. (Color online) Normalized resonance signal ζ of the Mn I ground and metastable state transitions as a function of the MIVOC charge temperature.

TABLE VII. Atomic charge-exchange cross sections populating the ${}^6S_{5/2}$ and ${}^8P_{9/2}$ states in Mn I.

Level	Direct (10^{-15} cm^2)	Including feeding (10^{-15} cm^2)
${}^6S_{5/2}$	2.02	5.71
${}^8P_{9/2}$	3.62	4.63

The relative population of the metastable state to the ground state including feeding from excited states was found to be

$$\frac{\zeta_{\text{metastable,calc}}}{\zeta_{\text{ground,calc}}} = \frac{4.63}{5.71} = 0.81, \quad (11)$$

in agreement with the relative population from the CLS measurements given in Eq. (10).

The large population of the ground state compared to that of the metastable state is due to the high number of excited electronic states which promptly depopulate to the ground state, even though the cross section to directly populate the metastable state is 45% larger than that of the ground state.

V. SUMMARY

Collinear laser spectroscopy was performed on neutral ${}^{55}\text{Mn}$ and ${}^{56}\text{Fe}$. Ion beams of Fe^+ and Mn^+ were generated by electron ionization of gaseous ferrocene and manganocene. The ions were accelerated to 15 keV and neutralized via charge-exchange reactions with a Na vapor. A long-lived

metastable state at an energy of 2.319 09 eV above the ground state of Mn I was populated in the charge-exchange process and was investigated via laser probing. Laser excitation of the ground states in both Mn I and Fe I were studied as well. The deduced center-of-gravity transition frequencies along with the determined A and B hyperfine coupling constants agreed with literature values, where available.

Asymmetry in the laser-induced fluorescence line shape was reproduced using an asymmetric Voigt profile. The linewidth and asymmetry of the fluorescence profile from the Mn I metastable state were found to be narrower and more symmetric compared to the fluorescence following the Mn I ground-state laser excitation. The relative populations of the Mn I metastable state compared to that of the ground state following charge exchange with a Na vapor was found to be 0.7 ± 0.3 . The theory of Rapp and Francis gives 0.81 and agreed with the present result. In the calculation, the cross section for the direct charge exchange to the metastable state is 45% larger than that of the ground state, which indicates that the contribution of feeding ground and metastable states from higher-energy excited states populated in the charge-exchange process is significant.

ACKNOWLEDGMENTS

This work was supported in part by National Science Foundation (NSF) Grant No. PHY-1102511. The authors thank S. Vinnikova, A. Schneider, and B. Johnson for their contributions to this work. A.K. acknowledges support from the NSF Graduate Research Fellowship Program.

-
- [1] K. R. Anton, S. L. Kaufman, W. Klempt, G. Moruzzi, R. Neugart, E. W. Otten, and B. Schinzler, *Phys. Rev. Lett.* **40**, 642 (1978).
- [2] S. Kaufman, *Opt. Commun.* **17**, 309 (1976).
- [3] M. Bacal and W. Reichelt, *Rev. Sci. Instrum.* **45**, 769 (1974).
- [4] M. Bacal, A. Truc, H. J. Doucet, H. Lamain, and M. Chretien, *Nucl. Instrum. Methods* **114**, 407 (1974).
- [5] N. Bendali, H. Duong, P. Juncar, J. S. Jalm, and J. Vialle, *J. Phys. B: At. Mol. Phys.* **19**, 233 (1986).
- [6] A. Klose, K. Minamisono, C. Geppert, N. Frömmgen, M. Hammen, J. Krämer, A. Krieger, C. Levy, P. Mantica, W. Nörtershäuser *et al.*, *Nucl. Instrum. Methods A* **678**, 114 (2012).
- [7] T. Brodzinski, H. Kronfeldt, J. Kropp, and R. Winkler, *Z. Phys. D: At. Mol. Clust.* **7**, 161 (1987).
- [8] A. Stancik and E. Brauns, *Vib. Spectrosc.* **47**, 66 (2008).
- [9] E. Gurnee and J. L. Magee, *J. Chem. Phys.* **26**, 1237 (1957).
- [10] D. Rapp and I. B. Ortenburger, *J. Chem. Phys.* **33**, 1230 (1960).
- [11] D. Rapp and W. E. Francis, *J. Chem. Phys.* **37**, 2631 (1962).
- [12] K. Minamisono, P. Mantica, A. Klose, S. Vinnikova, A. Schneider, B. Johnson, and B. Barquest, *Nucl. Instrum. Methods A* **709**, 85 (2013).
- [13] S. Vinnikova, Master's thesis, Michigan State University, 2011.
- [14] H. Koivisto, J. Ärje, and M. Nurmi, *Nucl. Instrum. Methods Phys. Res. B* **94**, 291 (1994).
- [15] H. Koivisto, J. Ärje, and M. Nurmi, *Rev. Sci. Instrum.* **69**, 785 (1998).
- [16] Stanford Research Systems, Inc., <http://www.thinksrs.com/>.
- [17] D. Lide, *CRC Handbook of Chemistry and Physics* (CRC Press LLC, Boca Raton, FL, 1999).
- [18] A. Kramida, Y. Ralchenko, J. Reader, and N. A. Team, *NIST Atomic Spectra Database (version 5.0)* (National Institute of Standards and Technology, Gaithersburg, MD, 2012), <http://physics.nist.gov/asd>.
- [19] A. E. Siegman, *Lasers* (University Science Books, Mill Valley, CA, 1986).
- [20] H. J. Metcalf and P. van der Straten, *Laser Cooling and Trapping* (Springer-Verlag, New York, 1999).
- [21] D. P. Dewangan, *J. Phys. B: At. Mol. Phys.* **6**, L20 (1973).
- [22] S. Davis, J. Wright, and L. Balling, *Phys. Rev. A* **3**, 1220 (1971).
- [23] H. Walther, *Z. Phys.* **170**, 507 (1962).
- [24] E. Handrich, A. Steudel, and H. Walther, *Phys. Lett. A* **29**, 486 (1969).
- [25] P. Lefèbvre, H. Garnir, and E. Biémont, *Astron. Astrophys.* **404**, 1153 (2003).
- [26] R. Blackwell-Whitehead, J. Pickering, and O. Pearse, *Astrophys. J. Sup. Ser.* **157**, 402 (2005).
- [27] R. Kurucz and B. Cell, *1995 Atomic Line Data* (Smithsonian Astrophysical Observatory, Cambridge, MA, 1995), <http://www.cfa.harvard.edu/amp/ampdata/kurucz23/sekur.html>.